Nano Research

Open Access

Research Article

Branched module-modified SN38 prodrug nanoassemblies for improved colorectal cancer therapy: Effectively balance efficacy and safety

Qing Wang[1,§], Shiyi Zuo[1,3,§], Shufang Zheng[1], Cuiyun Liu[1], Yaqiao Li[1], Jiayu Guo[1], Danping Wang[1], Shuo Wang[1], Wenjing Wang[1], Bowen Zhang[1], Minglong Huang[1], Xianbao Shi[4], Jin Sun[1,2], Zhonggui He[1,2], and Bingjun Sun[1,2] ✉

[1] *Department of Pharmaceutics, Wuya College of Innovation, Shenyang Pharmaceutical University, Shenyang 110016, China*
[2] *Joint International Research Laboratory of Intelligent Drug Delivery Systems, Ministry of Education, Shenyang Pharmaceutical University, Shenyang 110016, China*
[3] *School of Chemical Engineering, The University of Adelaide, Adelaide, SA 5005, Australia*
[4] *Department of Pharmacy, The First Affiliated Hospital of Jinzhou Medical University, Jinzhou 121001, China*
§ *Qing Wang and Shiyi Zuo contributed equally to this work.*

Cite this article: *Nano Research*, **2025**, *18*, 94907011. https://doi.org/10.26599/NR.2025.94907011

ABSTRACT: The clinical utility of irinotecan is restricted by individual variability in carboxylesterase expression. Direct administration of its active metabolite, 7-ethyl-10-hydroxycamptothecin (SN38), presents an appealing alternative due to its potent anti-tumor efficacy. However, the undesirable properties of SN38, such as poor water solubility and non-target toxicity, present significant hurdles to its clinical development. Prodrug nanoassemblies based on modular design strategy show promise in overcoming these challenges by enhancing drug delivery and selective activation. In modular design, the modification module plays a crucial role in improving the self-assembly capability of prodrugs. While current studies mainly focus on using straight aliphatic chains for prodrug design, branched aliphatic chains emerge as superior alternatives warranting further investigation. In this study, we selected 2-heptylundecanol ($BAlc_{18}$) as modification module to construct an SN38 prodrug. Through exquisite design, SN38-SS-$BAlc_{18}$ NPs integrated prominent properties in self-assembly capability, specific activation and biocompatibility, resolving the challenges of irinotecan and SN38, ultimately demonstrating excellent anti-tumor efficacy. This exploration enriched the design theory of prodrug nanoassemblies that can effectively balance safety and colorectal anti-tumor efficacy.

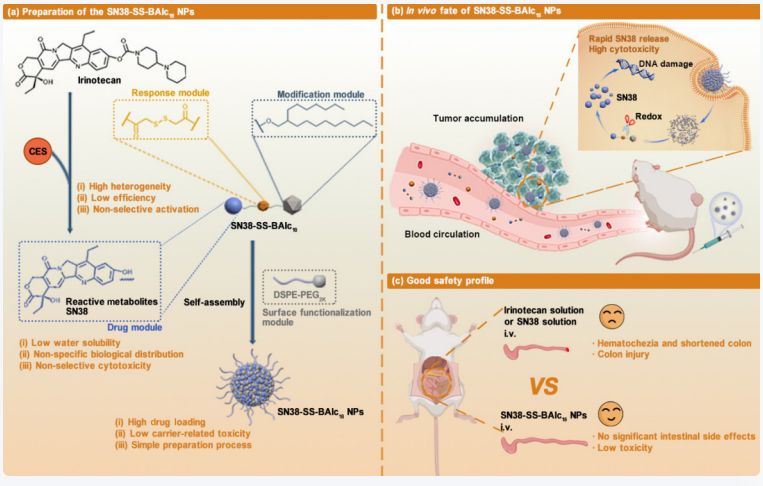

KEYWORDS: irinotecan, SN38, prodrug nanoassemblies, disulfide bonds, branched aliphatic chains

1 Introduction

Irinotecan (CPT-11, Campto®) demonstrates anticancer activity against a variety of solid tumors and has been approved for the clinical treatment of colorectal cancer [1, 2]. To exert its anti-tumor effect, irinotecan needs to be enzymatically converted by carboxylesterase (CES) into its active metabolite 7-ethyl-10-hydroxycamptothecin (SN38) [3, 4]. Unfortunately, the significant interindividual differences of carboxylesterase expression lead to a wide variation in patient outcomes, severely limiting efficacy of irinotecan [5–7]. Direct administration of SN38 can bypass this activation process, presenting an appealing alternative to provide potent tumor suppression efficacy [8]. Nonetheless, the extremely low water solubility (< 5 μg/mL) of SN38 poses obstacles to its *in vivo* delivery and clinical application [9]. Additionally, non-specific

Received: June 26, 2024; **Revised:** August 24, 2024
Accepted: August 28, 2024

✉Address correspondence to sunbingjun_spy@sina.com

biological distribution and non-selective cytotoxicity of SN38 can also lead to severe systemic toxicity [10, 11]. Such toxicity always leads to premature termination of the treatment or a reduction in dose intensity, thereby compromising therapeutic efficacy [7].

In addressing the limitations of the current irinotecan and SN38 treatments, prodrug nanoassemblies, which integrate the benefits of prodrug and nanoparticle (NP) drug delivery, provide a promising solution [12]. Unlike traditional preparation of nanoparticle drugs, prodrug nanoassemblies utilize the prodrugs themselves as nanocarriers, which have simple process, excellent reproducibility, and high feasibility for industrial production. The innovative self-assembly prodrug design improves the unfavorable physicochemical properties of chemotherapeutic drugs, allowing them to spontaneously assemble into nanoparticles in water [13, 14]. Besides, prodrugs are pharmacologically inert and necessitate the transformation to active parent drug to exert anti-tumor effect. Thus, by incorporating a specific response module that responds to tumor signaling can achieve tumor-responsive activation of prodrug, which in turn improves the activation efficacy and reduces off-target toxicity [15].

Based on the accumulative experience from our previous studies, we summarize the modular design strategy, which emphasizes prodrug nanoassemblies consist of four modules including drug module, response module, modification module, as well as surface functionalization module [16]. The drug module is centerpiece of the prodrug. For example, SN38 exhibits a hydroxyl group at the C-10 position, which is necessary for anti-tumor efficacy and can be harnessed for chemical modification [17–19]. The response module, as described above, enables prodrugs to specifically respond to specific signals of tumor microenvironment (TME) and selectively release the parent drug [20, 21]. Disulfide bond is widely used as a representative response module in response to TME which demonstrates much higher redox levels compared with normal cells [22–25]. The introduction of modification module helps to improve self-assembly ability of prodrugs [26]. Previous studies demonstrated that the self-assembly ability of branched chain modified prodrugs was superior to straight chain modified prodrugs, due to improved intermolecular interactions and steric hindrance. Additionally, branched chain modified prodrug nanoassemblies showed significant advantages in terms of pharmacokinetics, tumor accumulation and safety [27, 28]. Notably, current research on branched-chain fatty alcohols remains limited, necessitating further exploration. Furthermore, the surface functionalization module represented by DSPE-PEG_{2000} can enhances the stability of prodrug nanoassemblies, prolongs their blood circulation time and slow down elimination rate *in vivo* [29].

Therefore, SN38 was conjugated with 2-heptylundecanol ($BAlc_{18}$), a compound known for good biocompatibility, via a redox-responsive disulfide bond and the corresponding prodrug was abbreviated as SN38-SS-$BAlc_{18}$ (Fig. 1(a)). Using irinotecan solution and SN38 solution as controls, we systematically explored the self-assembly capacity and redox-responsive release profiles of SN38-SS-$BAlc_{18}$ NPs. Their pharmacokinetics, biodistribution, pharmacodynamics as well as biological safety were also clarified. Interestingly, SN38-SS-$BAlc_{18}$ NPs integrated prominent advantages in self-assembly capability, specific activation, and excellent biocompatibility, effectively addressing the existing challenges of irinotecan and SN38 while ultimately demonstrating improved anti-tumor efficacy (Figs. 1(b) and 1(c)). Through comprehensive exploration, we provided a new reference for the development of prodrug nanoassemblies, achieving a balance between safety and therapeutic efficacy in colorectal cancer treatment.

2 Results and discussion

2.1 Synthesis of SN38-SS-$BAlc_{18}$

The prodrug SN38-SS-$BAlc_{18}$ was synthesized by conjugating SN38 with $BAlc_{18}$ through α-disulfide bond in a yield of 58%, as shown in Fig. S1 in the Electronic Supplementary Material (ESM). The chemical structure was confirmed by ^{1}H-NMR and mass spectra (MS) (Figs. S2(a) and S2(b) in the ESM). The purity of the prodrugs was exceeded 99% according to HPLC analysis (Fig. S2(c) in the ESM).

2.2 The self-assembly ability of SN38-SS-$BAlc_{18}$

To evaluate the self-assembly ability of SN38-SS-$BAlc_{18}$, we prepared different concentrations of pure SN38-SS-$BAlc_{18}$ NPs without addition of surface functionalization module (referred to as nSN38-SS-$BAlc_{18}$ NPs), using one-step nanoprecipitation method (Fig. 2(a)). As shown in Fig. 2(b), SN38 was unable to form nanoparticles and precipitated even at a low concentration (0.5 mg/mL). In comparison, nSN38-SS-$BAlc_{18}$ NPs were successfully formed at concentrations of 0.5, 1, and 1.5 mg/mL. This can be attributed to its enhanced self-assembly ability after drug modification. These nanoparticles exhibited homogenous size distribution and their particle sizes gradually increased from 180 to 212 nm as the concentration increased. Based on the calculation of lg*P* of molecules (Fig. 2(c)), we found that hydrophobicity of SN38-SS-$BAlc_{18}$ was enhanced following the modification of SN38, which may provide a driving force for the self-assembly of prodrugs [30]. However, when the concentration exceeded a threshold limit, the intermolecular forces became excessively strong, thus resulting in the aggregation of drug molecules to precipitate [30].

The self-assembly mechanism of SN38-SS-$BAlc_{18}$ was further studied by using molecular docking simulations. As illustrated in Fig. 2(d), the self-assembly of SN38-SS-$BAlc_{18}$ was facilitated by multiple intermolecular forces, including π–π stacking, hydrogen bonding, and hydrophobic interactions. To gain further insight into the self-assembly interactions within SN38-SS-$BAlc_{18}$, nSN38-SS-$BAlc_{18}$ NPs (0.5 mg/mL) were incubated with sodium chloride (NaCl, 0.5 nM), urea (0.5 nM), and sodium dodecyl sulfate (SDS, 0.5 nM), which can destroy π–π stacking, hydrogen bonding, and hydrophobic interactions, respectively. As a result (Figs. 2(e)–2(g)), the hydrodynamic diameter of nSN38-SS-$BAlc_{18}$ NPs increased evidently after treatment with these destruction reagents. The TEM images further confirmed this result, showing that nSN38-SS-$BAlc_{18}$ NPs lost their nanostructures after co-incubation with destruction reagents for 2 h (Fig. S3 in the ESM). The above conclusions suggested that the π–π stacking, hydrogen bonding, and hydrophobic interactions are responsible for maintaining the stability of nSN38-SS-$BAlc_{18}$ NPs, as previously reported [31, 32].

2.3 Preparation and characterization of SN38-SS-$BAlc_{18}$ NPs

To improve colloidal stability and prolong blood circulation, PEGylated nanoassemblies was prepared for subsequent studies, which was named SN38-SS-$BAlc_{18}$ NPs (Fig. 3(a)). As shown in Fig. 3(b) and Table S1 in the ESM, SN38-SS-$BAlc_{18}$ NPs exhibited uniform spherical structures. The hydrodynamic diameter of SN38-SS-$BAlc_{18}$ NPs was approximately 100 nm with a narrow polymer dispersity index (PDI) (< 0.2), and the zeta potential was around

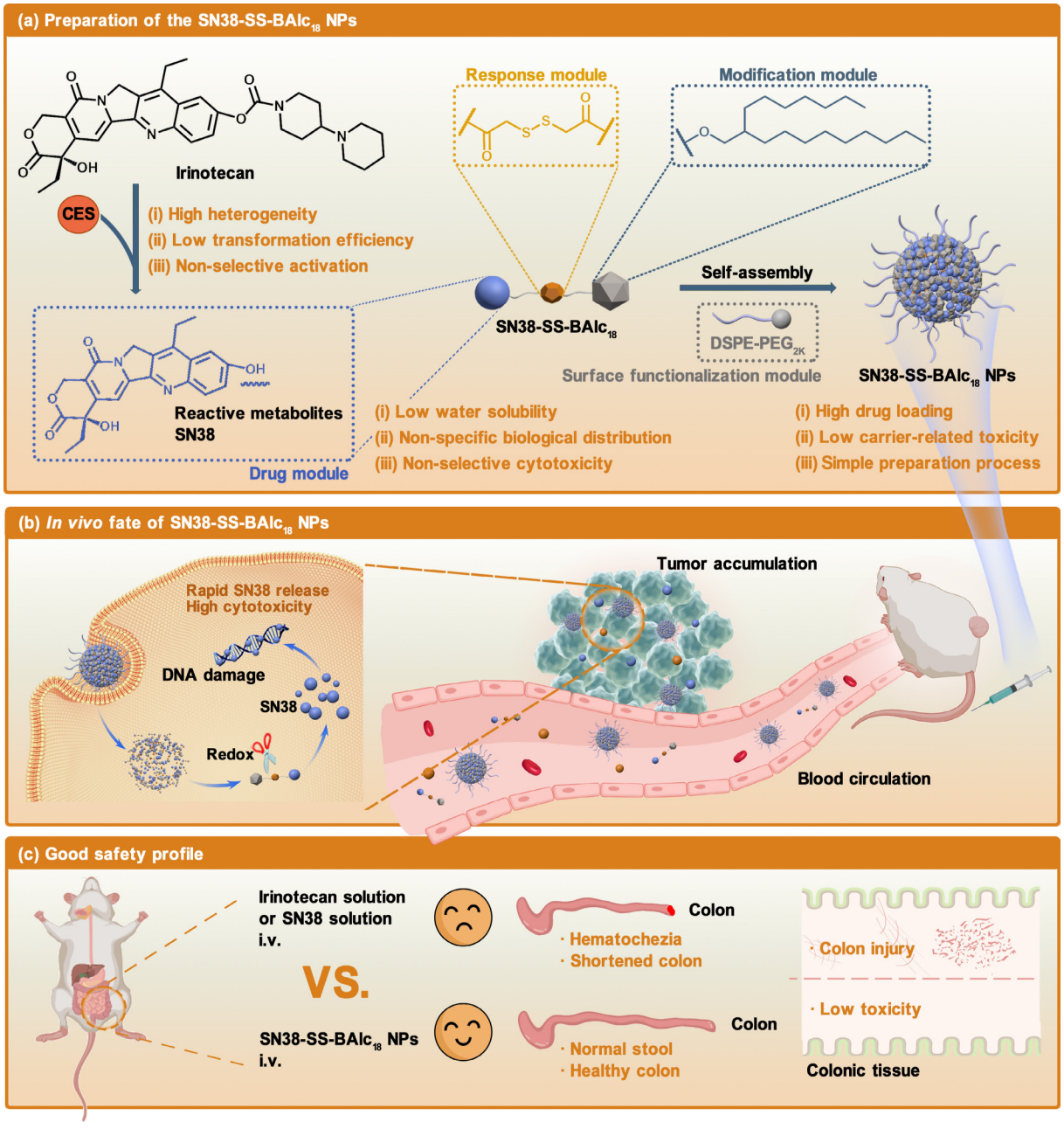

Figure 1 Schematic illustrations of SN38-SS-BAlc$_{18}$ NPs for safe and effective colorectal cancer therapy. (a) To address the challenges of irinotecan and SN38, SN38-SS-BAlc$_{18}$ NPs were constructed. (b) SN38-SS-BAlc$_{18}$ NPs exhibited a prolonged blood circulation and high tumor accumulation. At tumor site, SN38-SS-BAlc$_{18}$ NPs was specifically activated to release active components. (c) SN38-SS-BAlc$_{18}$ NPs avoided severe damage to colons caused by irinotecan and SN38.

−33 mV. Since no additional carrier materials were used, the prodrug nanoassemblies exhibited high drug loading capacity (38.8%, wt.%).

Then, the stability of the SN38-SS-BAlc$_{18}$ NPs was investigated under long-term storage conditions at 4, 25 and 37 °C. As depicted in Figs. 3(c)–3(e), the particle sizes of SN38-SS-BAlc$_{18}$ NPs remained stable over long periods. The interaction between prodrugs and DSPE-PEG$_{2000}$ were also investigated through molecular docking simulation. As shown in Fig. S4 in the ESM, there are multiple interactions between the prodrugs and DSPE-PEG$_{2000}$, such as hydrogen bonding and hydrophobic interactions, all of which played crucial roles in enhancing the colloidal stability of prodrug nanoassemblies. To investigate the colloidal stability of prodrug nanoassemblies in the normal physiological condition, SN38-SS-BAlc$_{18}$ NPs were incubated with PBS (pH 7.4) containing 10% FBS for 24 h. As a result (Fig. 3(f)), SN38-SS-BAlc$_{18}$ NPs showed negligible changes in particle size, indicating that prodrug nanoassemblies exhibited good stability during blood circulation and could prevent premature drug release.

To further illustrate the significance of prodrug nanoassemblies strategy, we compared the stability of SN38 solution with that of prodrug nanoassemblies. Due to the poor solubility of SN38, its solution was prepared using Cremophor EL and dimethyl sulfoxide (DMSO) as solubilizing agents, which may cause adverse reactions such as allergy. In contrast to the good stability of SN38-SS-BAlc$_{18}$ NPs, SN38 solution was less stable and precipitated within 2 h (Fig.

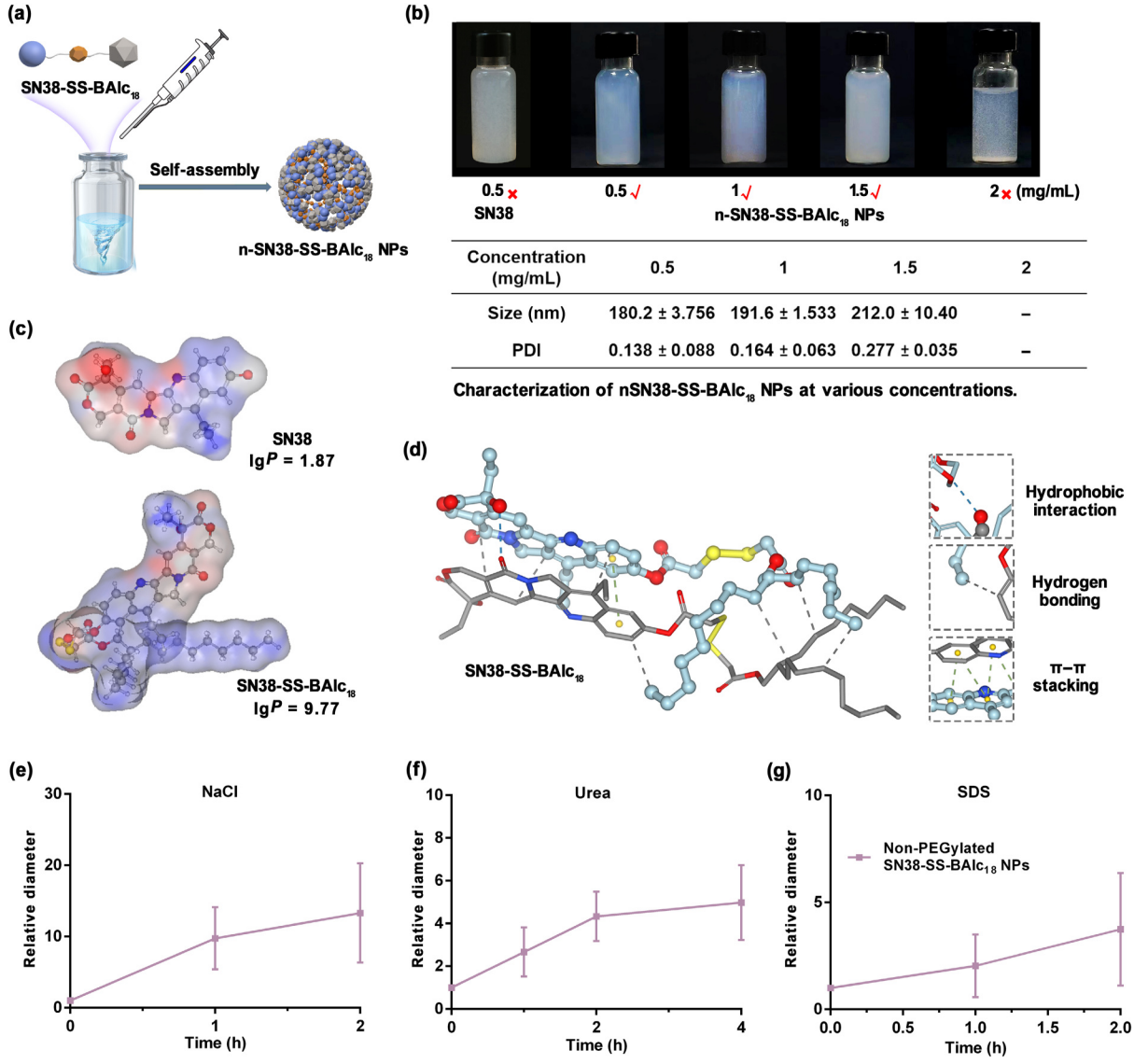

Figure 2 The self-assembly stability of SN38-SS-BAlc$_{18}$. (a) nSN38-SS-BAlc$_{18}$ NPs were prepared using one-step nanoprecipitation method. (b) Self-assembly performance of SN38 and SN38-SS-BAlc$_{18}$ at various concentrations. (c) The lg*P* value of SN38 and SN38-SS-BAlc$_{18}$. (d) Molecular docking simulations of SN38-SS-BAlc$_{18}$. Particle size change of SN38-SS-BAlc$_{18}$ NPs during co-incubation with (e) NaCl, (f) urea and (g) SDS. Data are presented as mean ± SD (n = 3).

3(g)). This instability suggested the fresh preparation of SN38 solution for administration was needed, which was inconvenient for clinical use and may pose potential risks. Overall, the prodrug strategy exhibited distinct advantages in improving adverse physicochemical properties and overcoming limitations in pharmaceutical formulations of SN38.

2.4 *In vitro* redox-responsive drug release

Given the unique responsiveness of disulfide bond to the tumor microenvironment [33], we explored the redox-responsive release profiles of SN38-SS-BAlc$_{18}$ NPs. The drug release in blank media was shown in Figs. 4(b) and 4(c). As a result, SN38 was merely released from SN38-SS-BAlc$_{18}$ NPs in blank media, which may reduce the undesirable drug release during blood circulation and thus mitigate systemic toxicity. By contrast, the interaction between SN38-SS-BAlc$_{18}$ NPs and GSH or H_2O_2 significantly enhanced the release of active SN38, reflecting the specific response of SN38-SS-BAlc$_{18}$ NPs to the redox state in tumors. As shown in Fig. 4(b), approximately 20% of SN38 was released from SN38-SS-BAlc$_{18}$ NPs under 5 mM H_2O_2 medium within 24 h.

With the increase of H_2O_2 concentration, more SN38 (about 26%) was released from SN38-SS-BAlc$_{18}$ NPs under 10 mM H_2O_2 medium. The H_2O_2-activated release mechanism of SN38-SS-BAlc$_{18}$ NPs was illustrated in Fig. 4(a). The presence of H_2O_2 led to the oxidation of disulfide bond, forming hydrophilic sulfone or sulfoxide group (Fig. S5(a) in the ESM). This increased hydrophilicity of the system and promoted ester bond hydrolysis, thereby releasing SN38.

As depicted in Fig. 4(c), SN38-SS-BAlc$_{18}$ NPs released 17% of SN38 under 0.1 mM GSH medium and 35% under 0.5 mM GSH medium within 24 h, similarly exhibiting a concentration-dependent behavior. The GSH-activated mechanism was clarified in Fig. 4(a). Disulfide bond was cleaved under the attack of GSH, generating hydrophilic thiol intermediate SN38-SH and causing the detachment of modification chain. This greatly increased hydrophilicity of the SN38 intermediate, allowing for easier drug

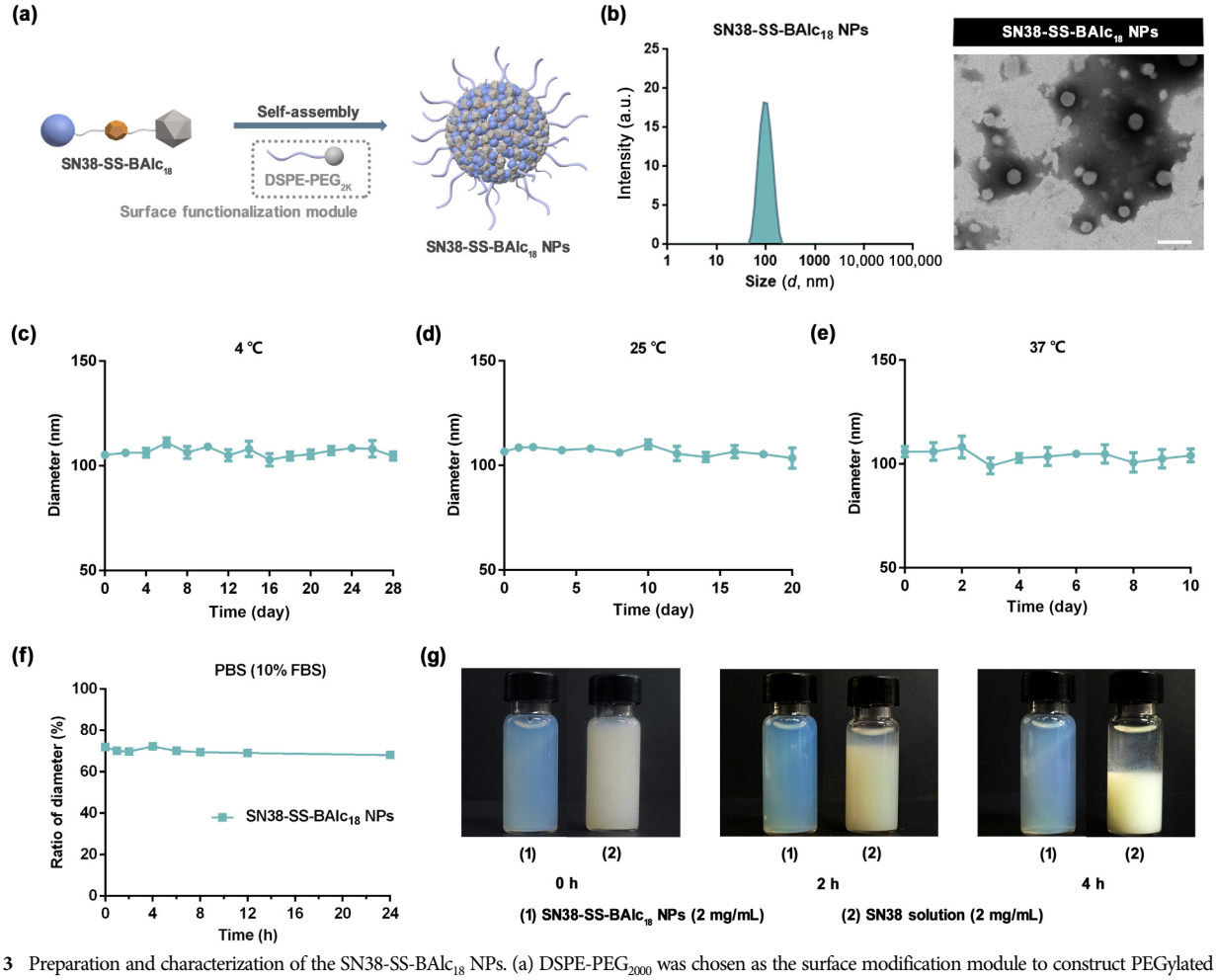

Figure 3 Preparation and characterization of the SN38-SS-BAlc$_{18}$ NPs. (a) DSPE-PEG$_{2000}$ was chosen as the surface modification module to construct PEGylated SN38-SS-BAlc$_{18}$ NPs. (b) Size distribution and TEM image of PEGylated SN38-SS-BAlc$_{18}$ NPs. Scale bar = 200 nm. The particles sizes of SN38-SS-BAlc$_{18}$ NPs remained stable for (c) 28 days at 4 °C, (d) 20 days at 25 °C, and for (e) 10 days at 37 °C. (f) Colloidal stability of SN38-SS-BAlc$_{18}$ NPs incubated with PBS (pH 7.4, containing 10% of FBS) for 24 h. (g) The stability of SN38-SS-BAlc$_{18}$ NPs and SN38 solution at 25 °C. Data are presented as mean ± SD (n = 3).

release from SN38-SS-BAlc$_{18}$ NPs under reduction conditions compared to oxidation conditions. Confirmation of reduction process was shown in Fig. S5(b) in the ESM.

To further demonstrate the superiority of the disulfide bond conjugated prodrug nanoassemblies, the drug release of SN38 solution and irinotecan solution were also evaluated. In contrast to the smart drug release behavior of SN38-SS-BAlc$_{18}$ NPs, SN38 solution consistently existed in the form of active SN38, which posed a great safety concern (Fig. S6 in the ESM). By comparison, irinotecan solution hardly released SN38 in response to redox stimulation, while its enzymatic release was inefficient as described previously [34].

2.5 *In vitro* anti-tumor therapy

Then, the impact of SN38-SS-BAlc$_{18}$ NPs, SN38 solution, and irinotecan solution on CT26 cells, including cellular uptake, intracellular release and cytotoxicity, were investigated. As depicted in Fig. 5(a), SN38 solution showed rapid cellular uptake into cells due to the passive diffusion mechanism [35, 36].

Besides, SN38 solution directly presented active SN38 to cells, therefore effectively inducing tumor cell death and exhibiting strong cytotoxicity (Figs. 5(c) and 5(d), and Table S2 in the ESM). As for irinotecan solution, it exhibited poor cell uptake compared to SN38 solution, due to its more hydrophilic property prevented the passage through hydrophobic cell membranes. The lower conversion rate dependent on carboxylesterase activation also prevented intracellular conversion of irinotecan to SN38 [34]. Thus, only a minimal amount of SN38 was released from irinotecan solution, leading to diminished cellular toxicity (Figs. 5(b) and 5(c), and Table S2 in the ESM). In contrast to the poor intracellular conversion ratio and drug release of irinotecan, SN38-SS-BAlc$_{18}$ NPs could rapidly release a large amount of SN38. Thus, despite their lower cellular uptake due to the PEG-modification, SN38-SS-BAlc$_{18}$ NPs exhibited potent cytotoxicity against CT26 cells. We further examined the cytotoxicity of SN38-SS-BAlc$_{18}$ NPs on 4T1 cells (Fig. 5(e) and Table S2 in the ESM), and the results were consistent of that on CT26 cells, in the following order of SN38 solution > SN38-SS-BAlc$_{18}$ NPs > irinotecan solution. We further evaluated the chemical stability of SN38-SS-BAlc$_{18}$ NPs in cell culture medium. As depicted in Fig. S7 in the ESM, only 9% of the prodrugs degraded within 48 h in blank culture medium, demonstrating that the cytotoxicity of SN38-SS-BAlc$_{18}$ NPs was primarily attributed to the active parent drug degraded by prodrugs under intracellular redox environment.

In addition, the cytotoxicity of SN38-SS-BAlc$_{18}$ NPs on normal cells L929 was also investigated. Although SN38 solution showed

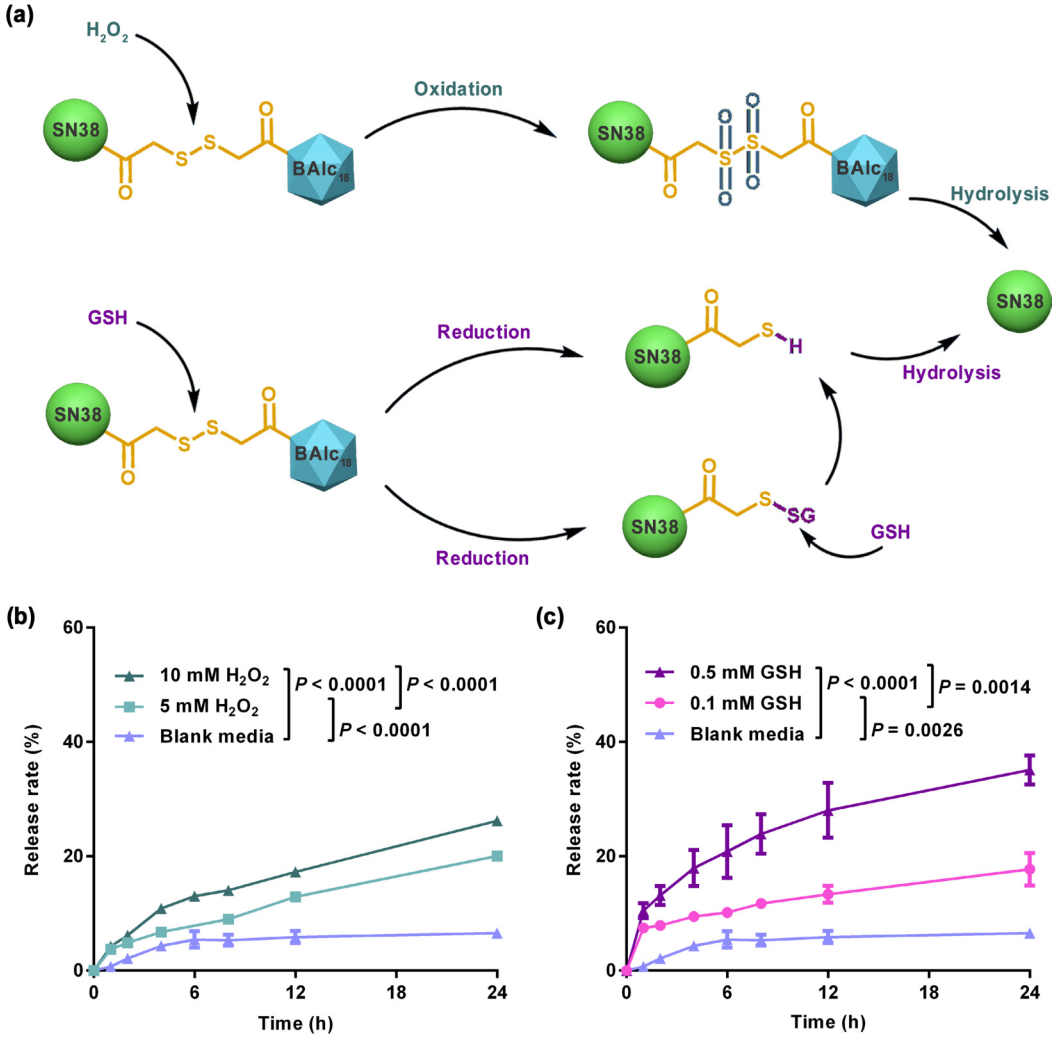

Figure 4 *In vitro* reduction-responsive drug release and mechanisms. (a) Mechanisms of the redox-responsive release of SN38-SS-$BAlc_{18}$ NPs. The *in vitro* release profiles of SN38 from SN38-SS-$BAlc_{18}$ NPs in blank media without any redox stimulation, as well as in various concentrations of (b) H_2O_2 and (c) GSH. Data are presented as the mean ± SD (n = 3). Statistical analysis was performed using two-tailed t-tests.

advantages in inhibiting tumor cells growth, its nonspecific effects also resulted in significant toxicity to normal cells. In contrast, SN38-SS-$BAlc_{18}$ NPs exhibited lower cytotoxicity against L929 cells (Fig. 5(f)). The selectivity index (SI) value was commonly employed as an indicator to assess the safety of chemotherapeutic drugs, specifically evaluating their selectivity towards tumor cells versus normal cells. As shown in Table S3 in the ESM, the SI value of SN38 solution and irinotecan solution were lower than that of SN38-SS-$BAlc_{18}$ NPs. This observation suggested that SN38-SS-$BAlc_{18}$ NPs could differentiate tumor cells from normal cells, significantly reducing the toxicity of SN38 towards normal cells and demonstrating favorable safety profiles (Fig. 5(g)).

2.6 *In vivo* pharmacokinetic study and biodistribution

In vitro hemolysis testing can provide valuable information about the hemocompatibility for *in vivo* experiments, therefore, it was performed on SN38 solution, irinotecan solution and SN38-SS-$BAlc_{18}$ NPs. As depicted in Fig. S8 in the ESM, SN38 solution exhibited mild hemolysis with a hemolysis rate of 5.1%, indicating a certain level of blood toxicity. This phenomenon could be attributed to the solubilizer Cremophor EL in SN38 solution [37]. In contrast, SN38-SS-$BAlc_{18}$ NPs showed a significantly lower hemolysis effect than free SN38 with a hemolysis rate of only 3% and demonstrated a good safety profile for intravenous administration.

The pharmacokinetic profiles of SN38 solution, irinotecan solution, and SN38-SS-$BAlc_{18}$ NPs were investigated in Sprague-Dawley rats. After intravenous administration, SN38 solution exhibited rapid clearance from the bloodstream, with the mean residence time (MRT) of merely 0.688 h (Fig. 6(b) and Table S4 in the ESM). As a hydrophilic prodrug of SN38, irinotecan exhibited diminished affinity for plasma protein binding [38], thereby resulting in slower blood clearance. Therefore, the area under the curve (AUC) of total SN38 in irinotecan was approximately 12.9 times higher than that in SN38 solution. However, the presence of abundant carboxylesterase in the bloodstream resulted in an 11% release of SN38 from irinotecan solution, potentially leading to hematotoxicity (Figs. 6(a)–6(c), and Table S4 in the ESM). In comparison to the two solutions, SN38-SS-$BAlc_{18}$ NPs exhibited a significantly prolonged blood circulation time of SN38. The AUC of total SN38 in SN38-SS-$BAlc_{18}$ NPs was approximately increased 750 times compared to that of SN38 solution and 58 times compared to that of irinotecan solution, which can be attributed to the excellent colloidal stability of SN38-SS-$BAlc_{18}$ NPs. Most

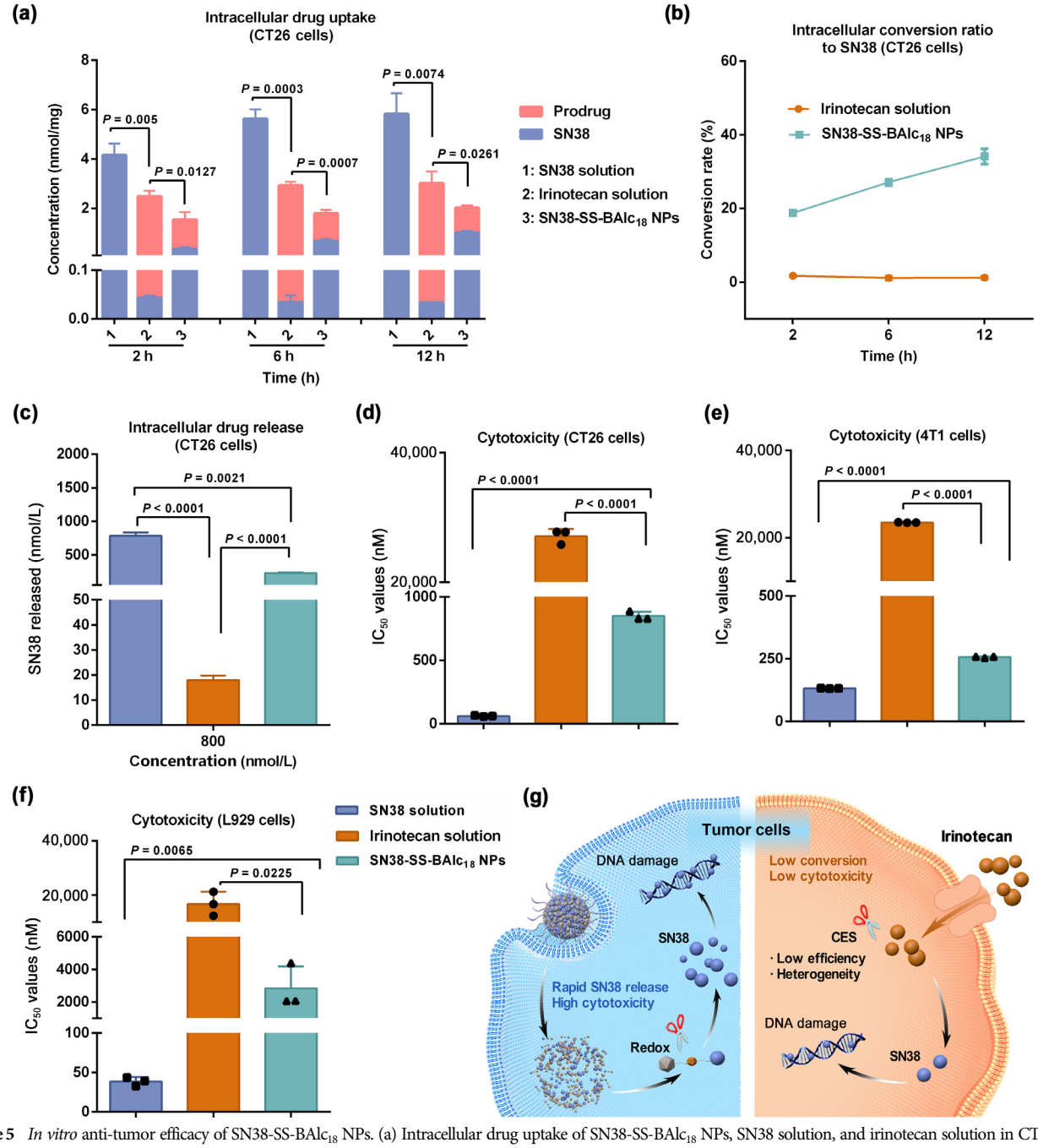

Figure 5 *In vitro* anti-tumor efficacy of SN38-SS-BAlc$_{18}$ NPs. (a) Intracellular drug uptake of SN38-SS-BAlc$_{18}$ NPs, SN38 solution, and irinotecan solution in CT26 cells was quantified using LC–MS–MS at 2, 6, and 12 h. (b) Intracellular conversion ratio of SN38-SS-BAlc$_{18}$ NPs and irinotecan solution to active metabolite SN38 by CT26 cells. (c) Intracellular drug release of SN38-SS-BAlc$_{18}$ NPs, SN38 solution and irinotecan solution in CT26 cells. IC$_{50}$ values (nM) of SN38-SS-BAlc$_{18}$ NPs, SN38 solution and irinotecan solution against tumor cells, including (d) CT26 cells and (e) 4T1 cells, and (f) normal L929 cells. (g) Cytotoxicity of SN38-SS-BAlc$_{18}$ NPs and irinotecan solution on tumor cells. Data are presented as mean ± SD (n = 3). Statistical analysis was performed using two-tailed t-tests.

importantly, only 0.8% of free SN38 was released from SN38-SS-BAlc$_{18}$ NPs (Figs. 6(a)–6(c), and Table S4 in the ESM), indicating that SN38-SS-BAlc$_{18}$ NPs prevented undesired drug exposure in blood circulation, thereby mitigating the hematological toxicity associated with SN38.

The biodistribution and tumor accumulation of SN38-SS-BAlc$_{18}$ NPs in CT26 tumor-bearing Balb/C mice were investigated using LC–MS–MS. As shown in Fig. 6(d) and Fig. S9 in the ESM, following intravenous administration of SN38 solution, SN38 was rapidly distributed into tumor and major organs at 1 h and cleared quickly due to unfavorable pharmacokinetic profiles. irinotecan solution also distributed rapidly throughout the main body tissues and was gradually converted into SN38, especially in liver where carboxylesterase is predominantly localized [6]. The resulting accumulation of SN38 may potentially induce hepatic damage. Compared to SN38 solution and irinotecan solution, SN38-SS-BAlc$_{18}$ NPs exhibited significantly higher tumor accumulation, especially at 4 h. The percentages of tumor accumulation at 24 h was further calculated for SN38-SS-BAlc$_{18}$ NPs and two solutions, yielding consistent results (Table S5 in the ESM). SN38-SS-BAlc$_{18}$

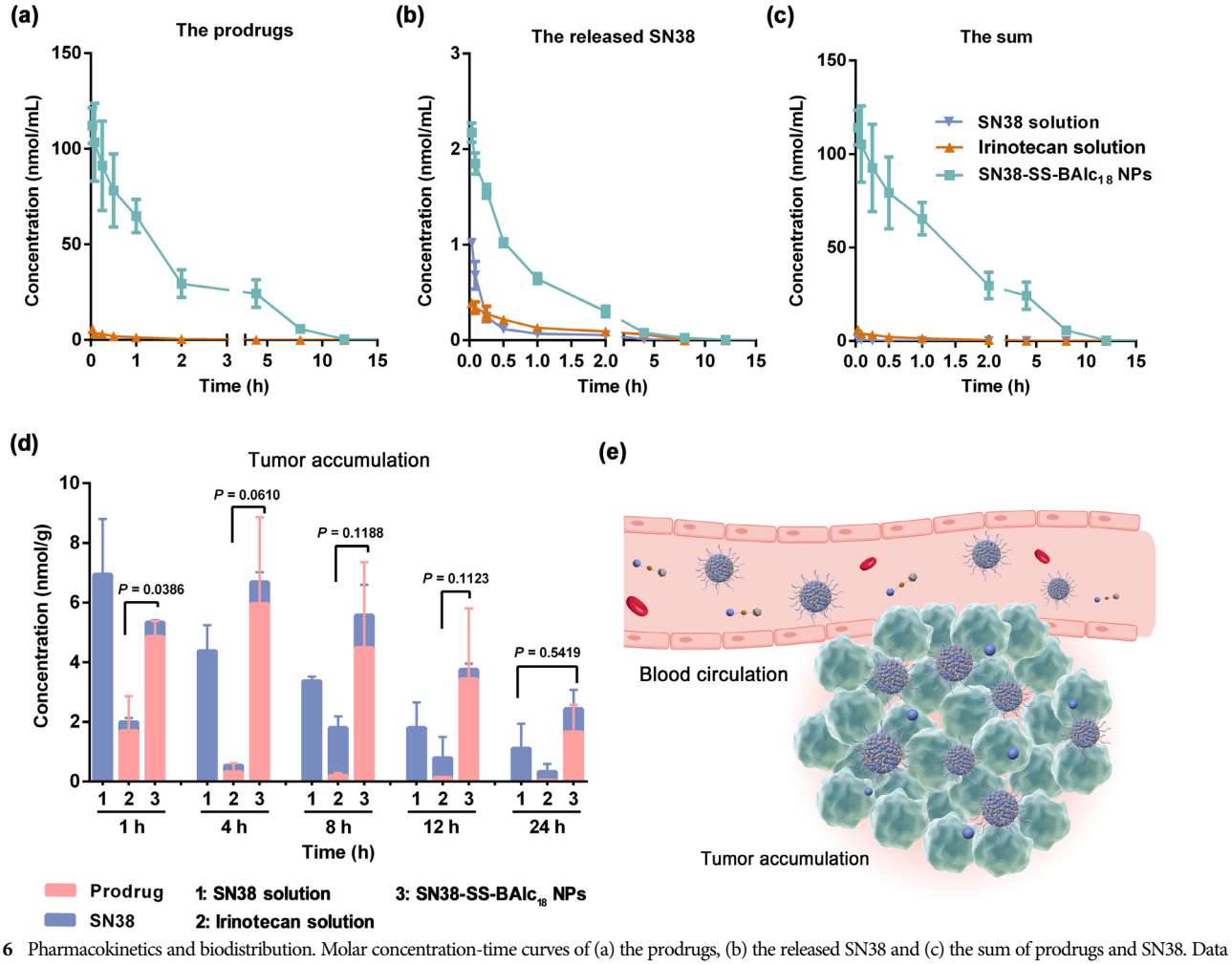

Figure 6 Pharmacokinetics and biodistribution. Molar concentration-time curves of (a) the prodrugs, (b) the released SN38 and (c) the sum of prodrugs and SN38. Data are presented as the mean ± SD (n = 4). (d) Quantitative results of tumor accumulation at 1, 4, 8, 12 and 24 h by LC-MS-MS. Data are presented as the mean ± SD (n = 3). (e) SN38-SS-BAlc$_{18}$ NPs showed significant advantages in blood circulation time and tumor accumulation. Statistical analysis was performed using two-tailed t-tests.

NPs exhibited a higher tendency to accumulate at tumor site compared to two solutions. Phagocytosis by reticuloendothelial system (RES) facilitates the uptake of nanoparticles in both liver and spleen [39]. Nevertheless, SN38-SS-BAlc$_{18}$ NPs predominantly existed as prodrugs in normal tissues, reducing off-target toxicity. These results were consistent with the pharmacokinetic studies, demonstrating that SN38-SS-BAlc$_{18}$ NPs achieved longer blood circulation time and better tumor accumulation, which was crucial for anti-tumor therapy (Fig. 6(e)).

2.7 *In vivo* anti-tumor efficacy and safety assessment

Finally, the anti-tumor efficacy of SN38 solution, irinotecan solution and SN38-SS-BAlc$_{18}$ NPs at an intravenous dose of 3 mg/kg (equivalent to SN38) was investigated in xenograft CT26 tumor-bearing Balb/C mice (Fig. 7(a)).

Compared with the saline group, both SN38 solution and irinotecan solution inhibited tumor growth to some extent. However, their therapeutic effectiveness was limited by their rapid clearance and poor tumor accumulation, not to mention the unfavorable conversion efficiency of irinotecan (Fig. 7(b)). In contrast, SN38-SS-BAlc$_{18}$ NPs exhibited superior tumor inhibition efficacy compared to SN38 solution, despite exhibiting lower cytotoxicity *in vitro*. This enhanced antitumor effect can be attributed to their prolonged blood circulation time and increased tumor accumulation *in vivo*.

We also conducted a comprehensive analysis of the safety profiles of anti-tumor treatment. As a result, no significant weight loss observed in mice treated with any groups after receiving five treatments (Figs. 7(c) and 7(d)). Myelosuppression and hepatorenal function injury were the most common toxic effects of chemotherapy, hence we further performed blood routine and hepatorenal function examination of mice. As indicated by the results of hepatorenal function assessments (Fig. 7(e) and Fig. S10 in the ESM), SN38 solution-treated mice showed abnormal increases in AST activity, indicating signs of liver injury. Moreover, the levels of BUN and CRE were elevated in irinotecan solution group, suggesting that irinotecan solution may cause kidney damage in mice. In comparison, no obvious signs of systematic toxicity were observed in mice treated with SN38-SS-BAlc$_{18}$ NPs, suggesting that SN38-SS-BAlc$_{18}$ NPs not only had superior anti-tumor efficacy but also exhibited good safety profiles.

Delayed diarrhea caused by the active metabolite SN38 is the most serious adverse effect of irinotecan, leading to colon shortening as well as intestinal cell damage [40–42]. Therefore, the colonic status was further utilized as a biosafety evaluation parameter to further explore the biosafety of SN38-SS-BAlc$_{18}$ NPs in mice.

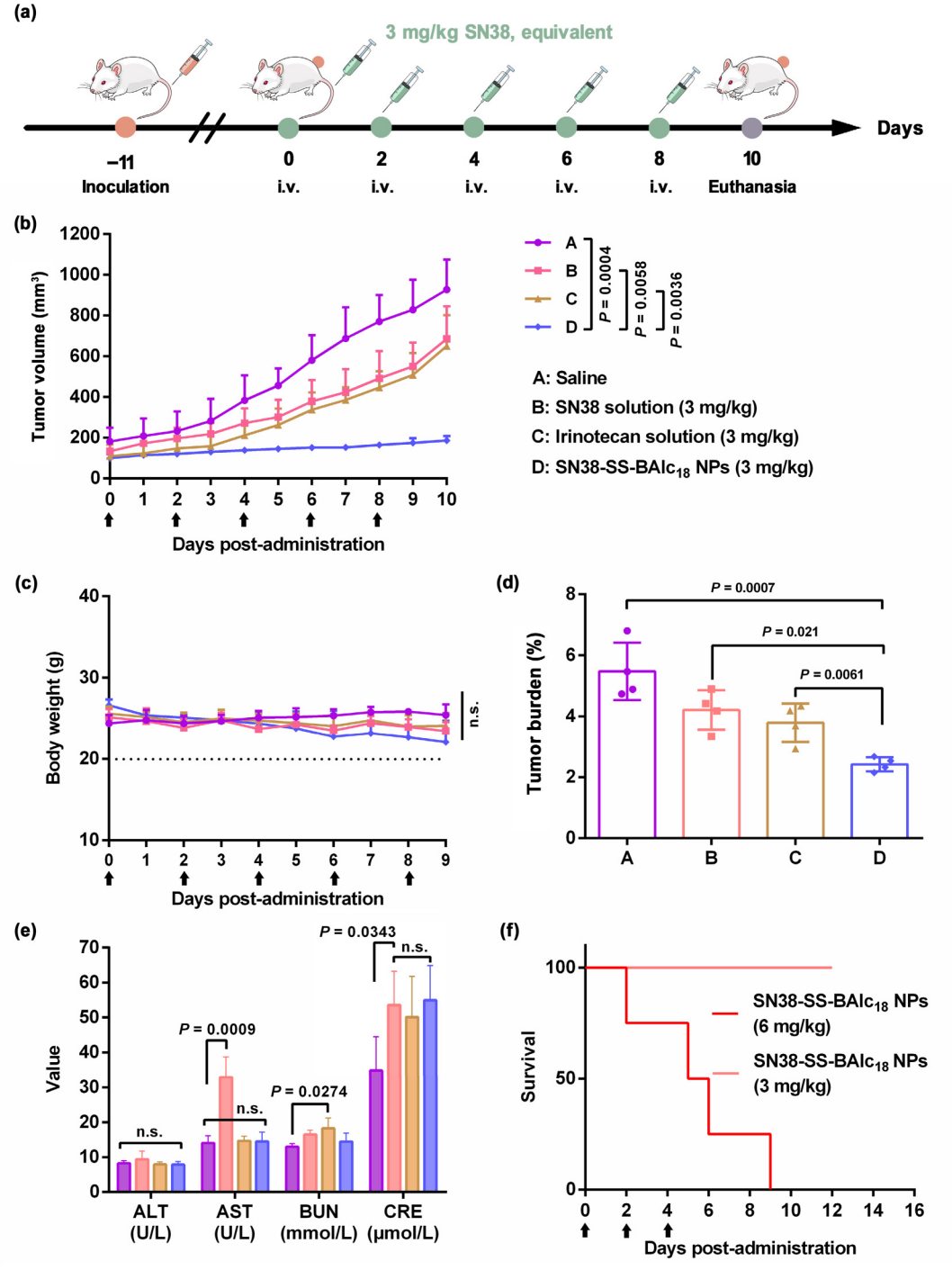

Figure 7 *In vivo* antitumor efficacy and tolerability of SN38-SS-BAlc$_{18}$ NPs. (a) CT26 xenograft tumor model was established with Balb/C mice and used to investigate the anti-tumor efficacy of SN38-SS-BAlc$_{18}$ NPs therapy. (b) Average tumor growth curves (TGCs). (c) Body weight changes. (d) Tumor burden. Data are presented as mean ± SD (n = 4). (e) Hepatorenal function parameters. ALT: alanine aminotransferase (U/L); AST: aspartate aminotransferase (U/L); BUN: blood urea nitrogen (mmol/L); CRE: creatinine (μmol/L). Data are presented as mean ± SD (n = 3). (f) Survival sample count of Balb/C mice during the treatment of SN38-SS-BAlc$_{18}$ NPs at high concentration and low concentration. Data are presented as mean ± SD (n = 6). Statistical analysis was performed using two-tailed t-tests.

Hematochezia symptoms were observed in SN38 solution-treated mice during the course of treatment. Besides, the colon length of the SN38 solution-treated mice were slightly shortened compared with the saline group, indicating that SN38 solution induced intestinal adverse effects (Fig. S11 in the ESM). As shown in Fig. S12 in the ESM, histopathological evaluation of colons was further performed by H&E staining [43, 44]. After intravenous administration of SN38 solution, obvious disappearance of intestinal gland structures was observed in mice, accompanied by considerable disarrangement and loosening of numerous intestinal glands. The observed severe colon damage may be attributed to the prolonged accumulation of SN38 in the intestine following enterohepatic circulation [36]. The high abundance of carboxylesterase in the intestine promotes the conversion of

irinotecan to SN38 [36]. After treatment with irinotecan, the colonic glands of mice also exhibited slight atrophy and villous damage. In comparison, colon tissue of saline- and SN38-SS-BAlc$_{18}$ NPs-treated mice remained intact biological structures, suggesting that SN38-SS-BAlc$_{18}$ NPs could protect the colon from damage caused by irinotecan and SN38.

Although SN38-SS-BAlc$_{18}$ NPs showed its unique advantages over irinotecan solution and SN38 solution in terms of safety and efficacy, its therapeutic window also attracted our attention. Thus, we further evaluated the safety profiles of higher doses of SN38-SS-BAlc$_{18}$ NPs, aiming to provide a more comprehensive evaluation. CT26-bearing Balb/C mice were treated with a higher dose of 6 mg/kg, and the corresponding results were shown in Fig. 7(f). In comparison to low-dose treatment, administration of high-dose SN38-SS-BAlc$_{18}$ NPs resulted in adverse effects in mice, including significant weight loss and hematochezia. This phenomenon suggested that although the therapeutic window of SN38 has been expanded by SN38-SS-BAlc$_{18}$ NPs through the modular prodrug design, constant attention is still required for toxicity and dose intensity. This highlights the necessity for precise medication in clinical practice to ensure a balance between safety and efficacy.

3 Conclusions

In this work, we designed and synthesized the SN38 prodrug by conjugating SN38 with 2-heptandecol via disulfide bond. We found that SN38-SS-BAlc$_{18}$ showed unique self-assembly capability, which significantly improving adverse physicochemical properties and overcoming pharmaceutical limitations of SN38. The introduction of the disulfide bond endowed with SN38-SS-BAlc$_{18}$ NPs the redox-responsive release profiles and excellent selectivity against tumor cells. Additionally, SN38-SS-BAlc$_{18}$ NPs prevented exposure of SN38 from irinotecan caused by carboxylesterase in blood circulation and thus improved hematological safety of SN38. Besides, SN38-SS-BAlc$_{18}$ NPs significantly prolonged blood circulation and consequently improved tumor accumulation, which was crucial for its anti-tumor efficacy. With excellent colloidal stability, prolonged blood circulation, high tumor accumulation and specific drug release, SN38-SS-BAlc$_{18}$ NPs showed significant anti-tumor efficacy in tumor-bearing mice while significantly reducing the systemic toxicity of SN38. In conclusion, SN38-SS-BAlc$_{18}$ NPs constructed by modular design strategy effectively achieved balance of efficacy and safety, providing an important reference for the rational design of prodrug nanoassemblies to achieve improved colorectal cancer therapy. Given that exquisite modular design brought different properties to prodrug nanoassemblies, the role of more types of modification modules or response modules in different drugs and their delivery systems deserves further exploration.

4 Experimental

4.1 Materials

SN38 was purchased from Macklin (Shanghai, China). Dithiodiglycolic acid was obtained by TCI Development Co. Ltd. (Shanghai, China). 1-Ethyl-3-(3-dimethyllaminopropyl) carbodiimide hydrochloride (EDCI), 4-dimethylaminopyrideine (DMAP), 1-Hydroxybenzotriazole (HOBT) and hydrogen peroxide (H_2O_2) were obtained from Aladdin Biochemical Technology Co. Ltd. (Shanghai, China). DSPE-PEG$_{2000}$ was purchased from AVT (Shanghai) Pharmaceutical Tech Co., Ltd. (Shanghai, China). Trypsin, phosphate-buffered saline (PBS), MTT, and cell culture medium were obtained by Meilun Biotech (Dalian, China). Fetal bovine serum (FBS) was supplied by Hyclone (Beijing, China). 96-Well plate, 24-well plate and 12-well plate were obtained from NEST Biotechnology. Aspartate Aminotransferase (AST/GOT) Activity Assay Kit, Alanine Aminotransferase (ALT/GPT) Activity Assay Kit, Urea (BUN) Colorimetric Assay Kit, Creatine kinase assay kit were provided by Nanjing Jiancheng Bioengineering Institute. The other reagents mentioned in this work were of analytical or HPLC grade.

4.2 Synthesis and structure confirmation of SN38-SS-BAlc$_{18}$ prodrugs

Dithiodiglycolic acid was reacted in acetic anhydride for 2 h. After treated with methylbenzene, the obtained yellowish oily liquid was dissolved with anhydrous dichloromethane as a solvent. The heptyl undecanol and DMAP were dissolved in appropriate amounts of anhydrous DCM and added to the stirring system in slow drops and reacted for 12 h at room temperature. The crude product was purified by column chromatography (cyclohexane and ethyl acetate as elutriant) to yield intermediate HO-SS-BAlc$_{18}$ (70% yield).

The resulted intermediate HO-SS-BAlc$_{18}$ was dissolved in chloroform with the catalyst (EDCI, HOBT, DMAP) and activated by an ice bath for 2 h. SN38 dissolved in DMSO was subsequently added to the reaction system slowly and the reaction was stirred for 48 h at room temperature. The reaction process was monitored by TLC. The target product (SN38-SS-BAlc$_{18}$ prodrugs) were isolated and purified by preparative liquid chromatography (solid, about 58% yield).

4.3 Assembly mechanism of SN38-SS-BAlc$_{18}$

For the non-PEGylated nanoassemblies, prodrugs were dissolved in acetone and injected dropwise into spiritedly stirring deionized water [13]. And non-PEGylated nanoassemblies were used to confirm the self-assembly mechanism. Specifically, the non-PEGylated nanoassemblies were added to aqueous solutions of urea (500 nmol/L), sodium dodecyl sulfate (SDS, 500 nmol/L) and sodium chloride (500 nmol/L), respectively (1/20, v/v). The mixture was incubated in the constant temperature oscillator at 37 °C. Finally, the Zetasizer (Nano ZS, Malvern Co., UK) was used to measure the particle size and PDI of the non-PEGylated nanoassemblies. The dynamical ratio of sizes and count rate were measured by Zetasizer. The morphological changes of SN38-SS-BAlc$_{18}$ NPs were also examined by Transmission electron microscopy. The Yinfo Cloud Computing Platform (https://cloud.yinfotek.com) was used to perform the molecular simulations, while oil-water partition coefficients (lg*P*) were predicted by Marvin Sketch.

4.4 Preparation of SN38-SS-BAlc$_{18}$ NPs

For the PEGylated nanoassemblies, prodrugs and DSPE-PEG$_{2000}$ were premixed in acetone at the weight ratio of 4:1 and injected dropwise into spiritedly stirring deionized water.

4.5 Characterization of SN38-SS-BAlc$_{18}$ NPs

The prodrug nanoassemblies diluted by deionized water were applied to measure hydrodynamic diameters and Zeta potential using a Zetasizer (Nano ZS, Malvern Co., UK). The Yinfo Cloud

Computing Platform (https://cloud.yinfotek.com) was used to perform the molecular simulations.

The drug loading (DL) of SN38-SS-BAlc$_{18}$ NPs were calculated using equations: DL (%) = (M_{SN38} × $m_{prodrug}$/$M_{prodrug}$) / ($m_{prodrug}$ + $m_{DSPE\text{-}PEG2000}$), where M_{SN38}, $M_{prodrug}$, $m_{prodrug}$, $m_{DSPE\text{-}PEG2000}$ represent the molecular weight of SN38, the molecular weight of prodrug, the quality of prodrug, and the quality of DSPE-PEG$_{2000}$ in SN38-SS-BAlc$_{18}$ NPs, respectively.

Morphological study was set to observe the morphology of SN38 prodrug nanoassemblies by the instrument of Transmission electron microscopy (TEM, Hitachi, HT7700, Japan). Concisely, the prodrug nanoassemblies diluted by deionized water was dropped on a carbon-coated copper grid for 30 s and then the samples were stained with 1% phos-photungstic acid for an additional 30 s.

4.6 Storage stability and colloidal stability

The stability of PEGylated SN38 prodrug nanoassemblies was evaluated after being stored at 4 °C for 28 days, at room temperature for 20 days, and 10 days in a 37 °C shaker.

The PEGylated SN38 prodrug nanoassemblies (0.5 mg/mL) were mixed with phosphate buffer saline (PBS, pH 7.4) containing 10% fetal bovine serum (1/20, v/v) and incubated in the constant temperature oscillator at 37 °C for 24 h. The particle size of nanoassemblies was measured at the indicated time using Zetasizer (Nano ZS, Malvern Co., UK).

4.7 *In vitro* intelligent responsive drug activation

The *in vitro* redox release behavior of PEGylated nanoassemblies was investigated by using hydrogen peroxide and GSH as oxidant and reducing agents. PBS (pH 7.4) containing 30% ethanol (v/v) was used as the release medium and incubated in 37 °C oscillator after addition of PEGylated nanoassemblies and different concentrations of redox material. The concentrations of precursor residue were determined by HPLC (n = 3) at predetermined time points. The release profiles of SN38 solution and irinotecan solution in media containing GSH (0.5 mM) or H_2O_2 (10 mM) were investigated as controls. Moreover, to explain the redox release mechanism, the release intermediates were determined by LC-MS-MS (LCMS-8060, Shimadzu Co., Japan).

4.8 Cell culture

Mouse mammary carcinoma cells (4T1 cells), mouse colon cancer cells (CT26 cells), and mouse fibroblasts cells (L929 cells) were brought from the cell bank of Chinese Academy of Sciences (Beijing, China). CT26 cells and L929 cells were cultured in DMEM medium (MeilunBio) containing 10% FBS and 1% antibiotics. 4T1 cells were cultured in Gibco 1640 medium (MeilunBio) containing 10% FBS and 1% antibiotics. All cells were cultured in incubator (37 °C, 5% CO_2). The culture medium was replaced regularly.

4.9 Cytotoxicity assays

MTT assay was used to evaluate the antiproliferative activities of SN38 solution, irinotecan solution and SN38-SS-BAlc$_{18}$ NPs. Three tumor cells (4T1, CT26 cells) and one normal cells (L929 cells) were used. In brief, the cell suspension was diluted with fresh culture medium to a concentration of 2 × 10^4 cells/mL, then 200 μL of the diluted cell suspension was inoculated into a 96-well plate. After 24 h, the old culture medium was replaced with different concentrations of SN38 solution, irinotecan solution and SN38-SS-BAlc$_{18}$ NPs diluted with fresh culture medium. The cells added pure culture medium were used as the control group, and the wells without cells were the zero-adjusted wells (n = 3). After 48 h, 35 μL of MTT solution (5 mg/mL) was added to each well and incubated for 4 h at 37 °C. Subsequently, the MTT-containing medium was removed and 200 μL of DMSO was added to dissolve the resulting blue formazan crystals. The IC_{50} was calculated using GraphPad Prism 8.0. At the same time, the tumor selective index (SI) was calculated as the following formula: SI = IC_{50}, L929/IC_{50}, tumor cells.

4.10 Intracellular drug release

The CT26 cells were seeded in 24-well plates at a density of 1 × 10^5 cells per well and incubated for 24 h. Then, the fresh DMEM medium was used to dilute the concentration of SN38 solution, irinotecan solution and SN38-SS-BAlc$_{18}$ NPs at 800 nmol/L (SN38 equivalent concentrations). Subsequently, the medicated medium was added to the plates. The cells were incubated in a constant temperature incubator at 37 °C for 48 h after administration. After that, the cell culture medium and cells were collected, ultrasonically destroyed and centrifuged to obtain the supernatant. Finally, the concentration of SN38 in the supernatant was quantitatively analyzed by LC-MS-MS (LCMS-8060, Shimadzu Co., JPN). We also evaluated the stability of SN38-SS-BAlc$_{18}$ NPs in cell culture medium.

4.11 Hemolysis assay

Blood was collected from untreated rats via the orbital route, and centrifugated at 1200 r/min for 10 min. The blood cells in the bottom layer were washed and diluted with saline. Subsequently, the blood cell suspension was mixed with saline, Triton X-100, SN38 solution, irinotecan solution and SN38-SS-BAlc$_{18}$ NPs, and placed to oscillator (37 °C, 100 r/min) for 2 h. Samples treated with saline served as the negative control, while those treated with Triton X-100 acted as the positive control. After 10 min of centrifugation at 3000 r/min, the supernatant was collected to measure the absorbance using microplate reader, and the hemolysis percentage (HP%) was calculated by (As-An)/(Ap-An) × 100%. As, An and Ap respectively refer to the absorbance of the sample, negative control sample and positive control sample.

4.12 Animal studies

Male Balb/C mice and male Sprague-Dawley rats were taken good care based on the guidelines overviewed in the Guide for the Care and Use of Laboratory Animals. All the animals were given sterile water and rodent diet of clean grade. All the relevant works had got approval from the Institutional Animal Ethical Care Committee (IAEC) of Shenyang Pharmaceutical University.

4.13 *In vivo* pharmacokinetics

The pharmacokinetic characteristics of SN38 solution, irinotecan solution and SN38-SS-BAlc$_{18}$ NPs were evaluated in the male Sprague-Dawley rats (200–220 g). The Sprague-Dawley rats were randomly divided into 3 groups (n = 4) after fasting for 12 h. Then, SN38 solution, irinotecan solution and SN38-SS-BAlc$_{18}$ NPs (SN38 equivalent concentrations = 5 mg/kg) were administered intravenously. At the indicated time intervals, blood was collected from the posterior ocular venous cluster of rats. After centrifugation (1.3 × 10^4 rpm for 5 min), the rat plasma samples were obtained. To remove the protein in the plasma, the protein precipitation method was used. The concentration of SN38 and prodrugs was measured

by LC–MS–MS using acetonitrile containing 0.1% formic acid as the mobile phase. DAS 2.0 software was used to calculate the pharmacokinetic characteristics.

4.14 *In vivo* biodistribution

100 μL of CT26 cells suspension (2×10^6 cells/mL) was injected subcutaneously into the right back of Balb/C mice. When tumors grew to about 400 mm^3, tumor-bearing mice were randomly divided into 3 groups ($n = 3$). SN38 solution, irinotecan solution and SN38-SS-BAlc$_{18}$ NPs (10 mg/kg equivalent to SN38) were injected into mice via tail vein. Then at 1, 4, 8, 12 and 24 h after administration, mice in each group were sacrificed, and the heart, liver, spleen, lung, kidney and tumor tissues were isolated and weighed ($n = 3$). In addition, the content of prodrugs and free SN38 in each organ and tumors were determined using LC-MS-MS.

4.15 *In vivo* antitumor efficacy

The CT26 cells (2×10^6 cells per 100 μL) were injected subcutaneously into the right back of the male Balb/C mice to establish the tumor model. When the tumor reached about 100 mm^3, the mice were randomly divided into four groups (four animals for each group): (1) saline solution, (2) SN38 solution (3 mg/kg), (3) irinotecan solution (3 mg/kg, equivalent to SN38), (4) SN38-SS-BAlc$_{18}$ NPs (3 mg/kg, equivalent to SN38). Mice were administrated intravenously corresponding preparations by once at 1 day interval for a total of 5 doses. The long and short diameters of the tumors and the body weight of the mice were measured and recorded daily, and the tumor volume was calculated. The calculation method of tumor volume is: long diameter × short diameter × short diameter × 0.5. The mice were sacrificed two days after the last administration, and the tumor tissue was isolated, weighed and photographed. The tumor burden ((tumor weight/body weight) × 100%) was calculated.

4.16 *In vivo* safety evaluation

Following the pharmacodynamic study, the mice were sacrificed two days after the last administration, and blood samples were collected and centrifuged to obtain the serum for analyzing hepatic and renal function and blood routine examination.

Colonic tissue from each group of mice was isolated, photographed and measured the length of the colon, then washed with normal saline, preserved in 4% paraformaldehyde, and embedded sections of intestinal Swiss rolls were prepared and stained for observation.

4.17 Tolerance

The healthy male Balb/C mice were used to evaluate the tolerance of SN38-SS-BAlc$_{18}$ NPs. SN38-SS-BAlc$_{18}$ NPs were administered intravenously to Balb/C mice (6 mg/kg equivalent to SN38, $n = 6$). Mice were administrated intravenously corresponding preparations by once at 1 day interval for a total of 3 doses. The survival of all mice was recorded every day until the assay was terminated.

4.18 Statistical analysis

Analyses were conducted using GraphPad Prism 8.0, and data were calculated as the means ± SD. Statistical comparisons between groups were analyzed with Student's t-test (two-tailed). $P > 0.05$ was regarded as no significance (n.s.). $P \leq 0.05$ was considered statistically significant.

Electronic Supplementary Material: Supplementary material (further details of chemical synthesis routes and characterizations of SN38-SS-BAlc$_{18}$, pharmacokinetics, biodistribution results, blood routine examination and colon staining image of mice) is available in the online version of this article at https://doi.org/10.26599/NR.2025.94907011.

Data availability

All data needed to support the conclusions in the paper are presented in the manuscript and the ESM. Additional data related to this paper may be requested from the corresponding author upon request.

Acknowledgements

This work was supported by the National Natural Science Foundation of China (Nos. 82272151 and 82204318), Liaoning Revitalization Talents Program (No. XLYC2203083), and Shenyang Young and Middle-aged Science and Technology Innovation Talent Support Program (No. RC220389).

Declaration of competing interest

All the contributing authors report no conflict of interests in this work.

Author contribution statement

B. J. S.: Conceptualization, project administration, supervision. Q. W. and S. Y. Z.: Investigation, writing – original draft. S. F. Z., C. Y. L., and Y. Q. L.: Data curation. J. Y. G., D. P. W., and S. W.: Formal analysis. W. J. W., B. Z., and M. L. H.: Methodology. Z. G. H., X. B. S., and J. S.: Writing – review & editing. All authors have read and approved the final version of the manuscript.

Informed consent

Not applicable.

Ethics statement

All the relevant works had gotapproval from the Institutional Animal Ethical Care Committee(IAEC) of Shenyang Pharmaceutical University (ethical code: SYPU-IACUC-2022-0302-010).

Use of AI statement

None.

References

[1] Mollica, A.; Stefanucci, A.; Feliciani, F.; Cacciatore, I.; Cornacchia, C.; Pinnen, F. Delivery methods of camptothecin and its hydrosoluble analogue irinotecan for treatment of colorectal cancer. *Curr. Drug Deliv.* **2012**, *9*, 122–131.

[2] Bailly, C. Irinotecan: 25 years of cancer treatment. *Pharmacol. Res.* **2019**, *148*, 104398.

[3] Ramesh, M.; Ahlawat, P.; Srinivas, N. R. Irinotecan and its active metabolite, SN-38: Review of bioanalytical methods and recent update from clinical pharmacology perspectives. *Biomed. Chromatogr.* **2010**, *24*, 104–23.

[4] Arthur, D. E.; Uzairu, A. Molecular docking study and structure-based design of novel camptothecin analogues used as topoisomerase I inhibitor. *J. Chin. Chem. Soc.* **2018**, *65*, 1160–1178.
[5] Hatfield, M. J.; Umans, R. A.; Hyatt, J. L.; Edwards, C. C.; Wierdl, M.; Tsurkan, L.; Taylor, M. R.; Potter, P. M. Carboxylesterases: General detoxifying enzymes. *Chem.-Biol. Interact.* **2016**, *259*, 327–331.
[6] de Man, F. M.; Goey, A. K. L.; van Schaik, R. H. N.; Mathijssen, R. H. J.; Bins, S. Individualization of irinotecan treatment: A review of pharmacokinetics, pharmacodynamics, and pharmacogenetics. *Clin. Pharmacokinet.* **2018**, *57*, 1229–1254.
[7] Páez, D. Genetics and adverse events with irinotecan treatment: What do we know. *Pharmacogenomics* **2019**, *20*, 393–395.
[8] Si, J. X.; Zhao, X. B.; Gao, S.; Huang, D. S.; Sui, M. H. Advances in delivery of irinotecan (CPT-11) active metabolite 7-ethyl-10-hydroxycamptothecin. *Int. J. Pharm.* **2019**, *568*, 118499.
[9] Liu, Y. Q.; Li, W. Q.; Morris-Natschke, S. L.; Qian, K. D.; Yang, L.; Zhu, G. X.; Wu, X. B.; Chen, A. L.; Zhang, S. Y.; Nan, X. et al. Perspectives on biologically active camptothecin derivatives. *Med. Res. Rev.* **2015**, *35*, 753–789.
[10] Sriram, D.; Yogeeswari, P.; Thirumurugan, R.; Bal, T. R. Camptothecin and its analogues: A review on their chemotherapeutic potential. *Nat. Prod. Res.* **2005**, *19*, 393–412.
[11] Beretta, G. L.; Gatti, L.; Perego, P.; Zaffaroni, N. Camptothecin resistance in cancer: Insights into the molecular mechanisms of a DNA-damaging drug. *Curr. Med. Chem.* **2013**, *20*, 1541–1565.
[12] Li, G. T.; Jin, Q. H.; Xia, F. L.; Fu, S. W.; Zhang, X. B.; Xiao, H. Y.; Tian, C. T.; Lv, Q. Z.; Sun, J.; He, Z. G. et al. Smart stimuli-responsive carrier-free nanoassembly of SN38 prodrug as efficient chemotherapeutic nanomedicine. *Acta Mater. Med.* **2023**, *2*, 54–63.
[13] Ding, Y. Y.; Wang, Y. X.; Hu, Q. Y. Recent advances in overcoming barriers to cell-based delivery systems for cancer immunotherapy. *Exploration* **2022**, *2*, 20210106.
[14] Ma, X. Y.; Xing, R. R.; Yuan, C. Q.; Ogino, K.; Yan, X. H. Tumor therapy based on self-assembling peptides nanotechnology. *View* **2020**, *1*, 20200020.
[15] Zhang, B. W.; Liu, W. Y.; Liu, J. R.; Huang, M. L.; Li, Y. Q.; Zhao, E. W.; Zhang, L. R.; Shi, X. B.; Sun, J.; He, Z. G. et al. Rational engineering of cholesterol-modified prodrug nanoassemblies for improving the tumor selectivity and safety of mitoxantrone. *Fundam. Res*., in press, DOI: 10.1016/j.fmre.2024.06.006.
[16] Li, G. T.; Sun, B. J.; Zheng, S. Z.; Xu, L.; Tao, W. H.; Zhao, D. Y.; Yu, J.; Fu, S. W.; Zhang, X. B.; Zhang, H. T. et al. Zwitterion-driven shape program of prodrug nanoassemblies with high stability, high tumor accumulation, and high antitumor activity. *Adv. Healthc. Mater.* **2021**, *10*, 2101407.
[17] Bala, V.; Rao, S. S.; Boyd, B. J.; Prestidge, C. A. Prodrug and nanomedicine approaches for the delivery of the camptothecin analogue SN38. *J. Controlled Release* **2013**, *172*, 48–61.
[18] Liu, Y.; Piao, H. Y.; Gao, Y.; Xu, C. H.; Tian, Y.; Wang, L. H.; Liu, J. W.; Tang, B.; Zou, M. J.; Cheng, G. Comparison of two self-assembled macromolecular prodrug micelles with different conjugate positions of SN38 for enhancing antitumor activity. *Int. J. Nanomedicine* **2015**, *10*, 2295–2311.
[19] Dai, Y.; Qian, M.; Li, Y. Structural modification endows small-molecular SN38 derivatives with multifaceted functions. *Molecules* **2023**, *28*, 4931.
[20] Guo, X. S.; Cheng, Y.; Zhao, X. T.; Luo, Y. L.; Chen, J. J.; Yuan, W. E. Advances in redox-responsive drug delivery systems of tumor microenvironment. *J. Nanobiotechnol.* **2018**, *16*, 74.
[21] Jiang, J. L.; Cui, X. Y.; Huang, Y. X.; Yan, D. M.; Wang, B. S.; Yang, Z. Y.; Chen, M. R.; Wang, J. H.; Zhang, Y. N.; Liu, G. et al. Advances and prospects in integrated nano-oncology. *Nano Biomed. Eng.*. **2024**, *16*, 152–187.
[22] Liu, T.; Li, L. X.; Wang, S.; Dong, F. D.; Zuo, S. Y.; Song, J. X.; Wang, X.; Lu, Q.; Wang, H. L.; Zhang, H. T. et al. Hybrid chalcogen bonds in prodrug nanoassemblies provides dual redox-responsivity in the tumor microenvironment. *Nat. Commun.* **2022**, *13*, 7228.
[23] Gao, Y. L.; Zuo, S. Y.; Li, L. X.; Liu, T.; Dong, F. D.; Wang, X.; Zhang, X. B.; He, Z. G.; Zhai, Y. L.; Sun, B. J. et al. The length of disulfide bond-containing linkages impacts the oral absorption and antitumor activity of paclitaxel prodrug-loaded nanoemulsions. *Nanoscale* **2021**, *13*, 10536–10543.
[24] Sun, Y. X.; Wang, S. M.; Li, Y. Q.; Wang, D. P.; Zhang, Y.; Zhang, H. T.; Lei, H. R.; Liu, X. H.; Sun, J.; Sun, B. J. et al. Precise engineering of disulfide bond-bridged prodrug nanoassemblies to balance antitumor efficacy and safety. *Acta Biomater.* **2023**, *157*, 417–427.
[25] Yang, Y. X.; Zuo, S. Y.; Zhang, J. X.; Liu, T.; Li, X. M.; Zhang, H. T.; Cheng, M. S.; Wang, S. J.; He, Z. G.; Sun, B. J. et al. Prodrug nanoassemblies bridged by Mono-/Di-/Tri-sulfide bonds: Exploration is for going further. *Nano Today* **2022**, *44*, 101480.
[26] Zang, W. F.; Sun, Y. X.; Zhang, J. Y.; Hao, Y. Z.; Jin, Q. H.; Xiao, H. Y.; Zhang, Z.; Shi, X. B.; Sun, J.; He, Z. G. et al. Two-tailed modification module tuned steric-hindrance effect enabling high therapeutic efficacy of paclitaxel prodrug nanoassemblies. *Chin. Chem. Lett*., in press, DOI: 10.1016/j.cclet.2024.110230.
[27] Wang, D. P.; Du, C. Y.; Wang, S.; Li, L. X.; Liu, T.; Song, J. X.; He, Z. G.; Zhai, Y. L.; Sun, B. J.; Sun, J. Probing the role of connecting bonds and modifying chains in the rational design of prodrug nanoassemblies. *ACS Appl. Mater. Interfaces* **2022**, *14*, 51200–51211.
[28] Xu, H. Z.; Zuo, S. Y.; Wang, D. P.; Zhang, Y.; Li, W. X.; Li, L. X.; Liu, T.; Yu, Y. H.; Lv, Q. Z.; He, Z. G. et al. Cabazitaxel prodrug nanoassemblies with branched chain modifications: Narrowing the gap between efficacy and safety. *J. Controlled Release* **2023**, *360*, 784–795.
[29] Li, Y. Q.; Li, L. X.; Jin, Q. H.; Liu, T.; Sun, J.; Wang, Y. J.; Yang, Z. J.; He, Z. G.; Sun, B. J. Impact of the amount of PEG on prodrug nanoassemblies for efficient cancer therapy. *Asian J. Pharm. Sci.* **2022**, *17*, 241–252.
[30] Sánchez-Iglesias, A.; Grzelczak, M.; Altantzis, T.; Goris, B.; Pérez-Juste, J.; Bals, S.; Van Tendeloo, G.; Donaldson, S. H.; Chmelka, B. F.; Israelachvili, J. N. et al. Hydrophobic interactions modulate self-assembly of nanoparticles. *ACS Nano* **2012**, *6*, 11059–11065.
[31] Luo, C.; Sun, B. J.; Wang, C.; Zhang, X. B.; Chen, Y.; Chen, Q.; Yu, H.; Zhao, H. Q.; Sun, M. C.; Li, Z. B. et al. Self-facilitated ROS-responsive nanoassembly of heterotypic dimer for synergistic chemo-photodynamic therapy. *J. Controlled Release* **2019**, *302*, 79–89.
[32] Wang, X.; Li, L. X.; Wang, D. P.; Zuo, S. Y.; Liu, T.; Dong, F. D.; Zhang, X. B.; He, Z. G.; Sun, B. J.; Sun, J. Minor change in the length of carbon chain has a great influence on the antitumor effect of paclitaxel-fatty alcohol prodrug nanoassemblies: Small roles, big impacts. *Nano Res.* **2022**, *15*, 3367–3375.
[33] Wang, X.; Liu, T.; Huang, Y. T.; Dong, F. D.; Li, L. X.; Song, J. X.; Zuo, S. Y.; Zhu, Z. Y.; Kamei, K. I.; He, Z. G. et al. Critical roles of linker length in determining the chemical and self-assembly stability of SN38 homodimeric nanoprodrugs. *Nanoscale Horiz.* **2023**, *8*, 235–244.
[34] Rivory, L. P.; Bowles, M. R.; Robert, J.; Pond, S. M. Conversion of irinotecan (CPT-11) to its active metabolite, 7-ethyl-10-hydroxycamptothecin (SN-38), by human liver carboxylesterase. *Biochem. Pharmacol.* **1996**, *52*, 1103–1111.
[35] Smith, D. J.; Leal, L. G.; Mitragotri, S.; Shell, M. S. Nanoparticle transport across model cellular membranes: When do solubility-diffusion models break down. *J. Phys. D: Appl. Phys.* **2018**, *51*, 294004.
[36] Müller, B.; Kreuter, J. Enhanced transport of nanoparticle associated drugs through natural and artificial membranes—a general phenomenon. *Int. J. Pharm.* **1999**, *178*, 23–32.
[37] Pei, X. Y.; Luo, F. F.; Zhang, J.; Chen, W. L.; Jiang, C.; Liu, J.

Dehydroascorbic acids-modified polymer micelles target cancer cells to enhance anti-tumor efficacy of paclitaxel. *Sci. Rep.* **2017**, *7*, 975.

[38] Parvez, M. M.; Basit, A.; Jariwala, P. B.; Gáborik, Z.; Kis, E.; Heyward, S.; Redinbo, M. R.; Prasad, B. Quantitative investigation of irinotecan metabolism, transport, and gut microbiome activation. *Drug. Metab. Dispos.* **2021**, *49*, 683–693.

[39] Liu, T.; Choi, H.; Zhou, R.; Chen, I. W. RES blockade: A strategy for boosting efficiency of nanoparticle drug. *Nano Today* **2015**, *10*, 11–21.

[40] Paulík, A.; Nekvindová, J.; Filip, S. Irinotecan toxicity during treatment of metastatic colorectal cancer: Focus on pharmacogenomics and personalized medicine. *Tumori J.* **2020**, *106*, 87–94.

[41] Boeing, T.; Gois, M. B.; de Souza, P.; Somensi, L. B.; de Mello Gonçales Sant'Ana, D.; da Silva, L. M. Irinotecan-induced intestinal mucositis in mice: A histopathological study. *Cancer Chemother Pharmacol.* **2021**, *87*, 327–336.

[42] Kong, L. T.; Rong, L.; Wang, M. H. UGT1A1 genetic testing for irinotecan should be done before starting the treatment, rather than after the development of serious adverse drug reactions. *J. Coll. Phys. Surg. Pak.* **2022**, *32*, 1651–1652.

[43] Burke, T. G.; Bom, D. Campthotecin design and delivery approaches for elevating anti-topoisomerase I activities *in vivo*. *Ann. N. Y. Acad. Sci.* **2000**, *922*, 36–45.

[44] Al-kasspooles, M. F.; Williamson, S. K.; Henry, D.; Howell, J.; Niu, F. G.; Decedue, C. J.; Roby, K. F. Preclinical antitumor activity of a nanoparticulate SN38. *Invest New Drugs* **2013**, *49*, 871–880.